

A Dual-Parametric Finite Element Method for Cavitation in Nonlinear Elasticity

Yijiang Lian^a, Zhiping Li^{a,*}

^a*LMAM & School of Mathematical Sciences, Peking University,
Beijing 100871, P.R.China*

Abstract

A dual-parametric finite element method is introduced in this paper for the computation of singular minimizers in the two dimensional cavitation problem in nonlinear elasticity. The method overcomes the difficulties, such as the mesh entanglement and material interpenetration, generally encountered in the finite element approximation of problems with extremely large expansionary deformation. Numerical experiments show that the method is highly efficient in the computation of cavitation problems. Numerical experiments are also conducted on discrete problems without the radial symmetry to show the validity of the method to more general settings and the potential of its application to the study of mechanism of cavity nucleation in nonlinear elastic materials.

Keywords: dual-parametric finite element, cavitation, extremely large expansionary deformation, nonlinear elasticity, energy minimization, Picard iteration.

2000 MSC: 65N30, 74B20, 74G55, 74G65, 74M99, 74S05

1. Introduction

Nonlinear elastic materials can behave drastically differently from linear ones. One of the most significant phenomena, known as cavitation, is that the voids may develop in the material when tension exceeds certain critical level [2]. While the phenomenon can somehow be explained by pre-existing

*Corresponding author

Email addresses: sky_yjl@163.com (Yijiang Lian), lizp@math.pku.edu.cn (Zhiping Li)

deficiencies in the material growing into large voids as shown by Gent and Lindley [2] in 1958, a striking break through made by Ball [1] in 1982 showed that the cavitation phenomenon can also happen without the hypothesis of pre-existing deficiencies. In Ball's approach, one typically considers the problem of minimizing an elastic energy of the form

$$E(\mathbf{u}) = \int_{\Omega} W(\nabla \mathbf{u}(\mathbf{x})) d\mathbf{x} - \int_{\Omega} \mathbf{f} \cdot \mathbf{u} d\mathbf{x} - \int_{\Gamma_1} \mathbf{g} \cdot \mathbf{u} d\mathbf{x}, \quad (1.1)$$

where $\Omega \subset \mathbb{R}^d$, with $d = 2$ or 3 , is the reference configuration of the elastic body, $W : M_+^{3 \times 3} \rightarrow \mathbb{R}^+$ is the stored energy density function of the material and $M_+^{3 \times 3}$ denotes the 3×3 matrices with positive determinant, \mathbf{f} and \mathbf{g} are the body force and surface traction respectively, in a set of admissible deformations

$$\mathbb{U} = \{ \mathbf{u} \in W^{1,1}(\Omega; \mathbb{R}^d) \text{ is a bijection} : u|_{\Gamma_0} = u_0, \det \nabla \mathbf{u} > 0 \text{ a.e.} \}. \quad (1.2)$$

In the simplest setting, as is adopted in many literatures and will be adopted in the present paper, one has $\mathbf{f} = 0$ and $\mathbf{g} = 0$, Γ_1 is the boundary of the deficiencies which are pre-existing or produced after cavitation, Γ_0 is the rest of the boundary $\partial\Omega$, the boundary condition is given in the form

$$\mathbf{u}|_{\Gamma_0} = \lambda \mathbf{x} \quad (1.3)$$

with λ being sufficiently large, and the stored energy density is a polyconvex function [1] of the form

$$W(\mathbf{F}) = \kappa |\mathbf{F}|^p + h(\det \mathbf{F}), \mathbf{F} \in M_+^{3 \times 3}, p \geq 1, \quad (1.4)$$

where $\kappa > 0$ is a material constant, $|\cdot|$ denotes the Euclidean norm ($|\mathbf{A}|^2 = \text{trace}(\mathbf{A}^T \mathbf{A})$), and $h : (0, \infty) \rightarrow [0, \infty)$ is continuously differentiable, convex and satisfies

$$h(\delta) \rightarrow +\infty \text{ as } \delta \rightarrow 0, \text{ and } \frac{h(\delta)}{\delta} \rightarrow +\infty \text{ as } \delta \rightarrow +\infty.$$

Ball's theory is based on the fact that creation of cavities can be energetically favorable under certain circumstances. The gap between the deficiency model and the perfect (deficiency-free) model was closed by Sivaloganathan in 1986 [5], he proved that: the deficiency model solution would converge to

the perfect model solution, when the diameter of the initial deficiency approaches to zero. The result was later developed into a regularizing domain method [7], which provided a theoretical approach to obtain an approximate cavitation solution to the perfect model from the one to the deficiency model. Basically, these theoretical results are concerned with energy minimization in a restricted set of radially symmetric functions. However, there are examples showing that more sophisticated cavitations might be generally expected [9].

The cavitation phenomenon, including the cavity nucleation, growth and merge, has long being considered one of the key elements of the underline mechanisms of the fracture initiation and growth in nonlinear elastic materials, and mathematical modeling and numerical simulation have being expected to play a crucial rule in studying the cavitation phenomenon. However, due to its complexity, the analytical and numerical results on the solutions are mostly concentrated on the 1D problem reduced from radially symmetric models (for the numerical studies and the corresponding references see [13] and [10] among many others). To our knowledge, the first and the only 2D numerical simulation on cavitation appeared so far in the literature was given by Negrón-Marrero in 1986 [4], where a spectral-collocation method is applied. The work however did not stimulate further studies, probably because of the seemingly obvious limitations of applying to a more general settings.

Not as commonly would have been expected by many researchers, the result on the generally believed versatile finite element methods can be hardly found, if there is any, in the literature of cavitation computations. One of the main reasons that the finite element methods failed so far to successfully simulate the cavitation phenomenon is shown in Figure 1, where it is clearly seen that a triangular element $\triangle ABC$ of a piecewise affine interpolation of a small ring reverses its orientation after a sufficiently large expansion (see $\triangle A'B'C'$). The alternation of the orientation can be easily detected by the sign of the determinant of the deformation gradient. For example, for a radially symmetric deformation $\mathbf{u}(\mathbf{x}) = r(R)\frac{\mathbf{x}}{|\mathbf{x}|}$ of a ring, where $R = |\mathbf{x}|$ and $r = |\mathbf{u}|$, the determinant of the deformation gradient

$$\det \nabla \mathbf{u} = \frac{r(\varepsilon + \delta)[r(\varepsilon + \delta) \cos \frac{\pi}{m} - r(\varepsilon)]}{(\varepsilon + \delta)[(\varepsilon + \delta) \cos \frac{\pi}{m} - \varepsilon]}$$

can be negative, if r/R is sufficiently large.

In numerical simulations, the phenomenon would either prevent the small deficiency growing into large voids or cause mesh tanglement and produce

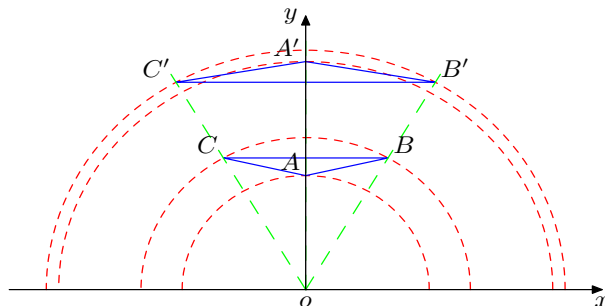
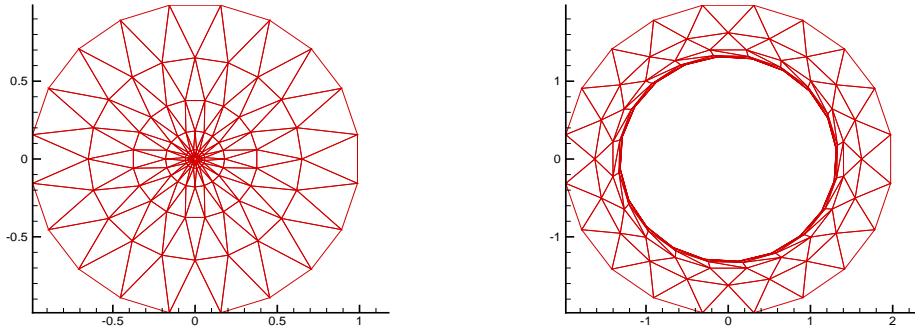


Figure 1: For a sufficiently large expansion of a small ring, the orientation of an affine element can be reversed.

physically unfeasible interpenetration numerical solutions. Although theoretically the difficulty can be somehow overcome by finely tuning the relationship between m , ϵ and δ , which will generally require to tremendously increase the degrees of freedom, the problem is that the numerical results heavily depend on the relations and there is no way to give a feasible relation without some a priori knowledge on the singularity of the cavitation. In addition, our numerical experiments show that the piecewise affine conforming finite element method is in general heavily mesh dependent and can lead to pseudo cavities of various radii. Furthermore, the piecewise affine conforming finite element method is found unstable on a theoretically feasible radially symmetric mesh and results in numerical solutions with either a clockwise or an anticlockwise screwed cavity (see Figure 2).

Recently, X. Xu and D. Henao reported their study on the nonconforming finite element method for the cavitation problem in a private communication [12]. They demonstrated that, on feasible meshes, the nonconforming finite element method combined with a penalty stabilizer allows a small deficiency growing into a sufficiently large void, however the interlacement of triangular elements near the void's boundary and the tricky determination of penalty strength seem to cause difficulties in convergence and approximation accuracy.

In the present paper, we develop a dual-parametric finite element method for the cavitation problem. The idea is to use properly chosen curved triangulations on the reference configuration and to use higher order base functions to construct the conforming finite element function space, so that even after extremely large expansionary deformation the curved triangular elements on a quite general mesh will still be able to preserve their orientation



(a) Initial radially symmetric mesh (b) A clockwise screwed numerical solution

Figure 2: Piecewise affine conforming finite element method is found unstable and may leads to screwed cavities.

and will not create mesh entanglement. Our numerical experiments show that the method is a great success. In fact, in an example with comparable 1D numerical results, of which the accuracy is theoretically guaranteed, our numerical experiments produce very accurate results with quite a small number of degrees of freedom, and in more sophisticated examples without radial symmetry the numerical results well match the theoretical expectations.

The rest of the paper is organized as follows. In Section 2, we introduce the dual-parametric curved triangular finite element, and develop an algorithm using the Picard iteration to solve the Euler-Lagrange equation of the discrete problem. In Section 3, numerical examples and results are presented and discussed. Finally, some conclusion remarks are made in Section 4.

2. Numerical Method

The aim of this section is to develop a finite element method to solve the Euler-Lagrange equation of the problem of minimizing the energy functional $E(\mathbf{u})$ in a properly defined admissible function space \mathbb{U} as described in Section 1.

2.1. The Euler-Lagrange equation

For $\mathbf{f} = 0$ and $\mathbf{g} = 0$, the Fréchet derivative of $E(\mathbf{u})$ can be derived as follows

$$\begin{aligned} \left\langle \frac{\partial E(\mathbf{u})}{\partial \mathbf{u}}, \mathbf{v} \right\rangle &= \left. \frac{dE(\mathbf{u} + s\mathbf{v})}{ds} \right|_{s=0} = \int_{\Omega_\varepsilon} D_F W(\nabla \mathbf{u}) : \nabla \mathbf{v} d\mathbf{x} \\ &= \sum_{i=1}^N \int_{\partial B_\varepsilon(c_i)} \mathbf{v} \cdot (D_F W(\nabla \mathbf{u}) \boldsymbol{\nu}) ds - \int_{\Omega} \operatorname{div}(D_F W(\nabla \mathbf{u})) \cdot \mathbf{v} d\mathbf{x}, \quad \forall \mathbf{v} \in \mathbb{U}_0, \end{aligned}$$

where Ω_ε is the domain of the reference configuration with ε a parameter for the size of the deficiencies $B_\varepsilon(c_i)$ geometrically centered at c_i , $i = 1, \dots, N$, for example $B_\varepsilon(a)$ can be a ball centered at a with radius ε , $\boldsymbol{\nu}$ denotes the unit interior normal to $\partial B_\varepsilon(c_i)$, that is the unit exterior normal to the corresponding part of $\partial\Omega_\varepsilon$, and where $\Gamma_0 = \partial\Omega_\varepsilon \setminus \cup_{i=1}^N \partial B_\varepsilon(c_i)$ denotes the outside boundary of the domain, and

$$\mathbb{U}_0 := \{ \mathbf{u} \in W^{1,1}(\Omega; \mathbb{R}^d) : u|_{\Gamma_0} = 0 \}.$$

Thus, the weak form of the Euler-Lagrange equation of the problem is given by

$$\sum_{i=1}^N \int_{\partial B_\varepsilon(c_i)} \mathbf{v} \cdot (D_F W(\nabla \mathbf{u}) \boldsymbol{\nu}) ds - \int_{\Omega} \operatorname{div}(D_F W(\nabla \mathbf{u})) \cdot \mathbf{v} d\mathbf{x} = 0, \quad \forall \mathbf{v} \in \mathbb{U}_0, \quad (2.5)$$

which leads to the following Euler-Lagrange equation:

$$\operatorname{div}(D_F W(\nabla \mathbf{u})) = \mathbf{0}, \quad \text{in } \Omega_\varepsilon, \quad (2.6)$$

$$D_F W(\nabla \mathbf{u}) \boldsymbol{\nu} = \mathbf{0}, \quad \text{on } \cup_{i=1}^N \partial B_\varepsilon(c_i), \quad (2.7)$$

$$\mathbf{u}(\mathbf{x}) = \mathbf{u}_0(\mathbf{x}), \quad \text{on } \Gamma_0. \quad (2.8)$$

In particular, for the stored energy density function given by (1.4), we have

$$D_F W(\nabla \mathbf{u}) = |\nabla \mathbf{u}|^{p-2} \nabla \mathbf{u} + h'(\det \nabla \mathbf{u}) \operatorname{adj} \nabla \mathbf{u}^T. \quad (2.9)$$

2.2. The dual-parametric finite element

Let \hat{T} be the reference triangular element as shown in Figure 3(a). For a given set of three points $a_i = (x_i, y_i)$, $1 \leq i \leq 3$, let (r_i, θ_i) be the corresponding polar coordinates, *i.e.* $x_i = r_i \cos \theta_i$ and $y_i = r_i \sin \theta_i$, we define a

polar coordinate parametric map $F_T : \hat{T} \rightarrow \mathbb{R}^2$ as

$$\begin{cases} r = (1 - \hat{x} - \hat{y})r_1 + \hat{x}r_2 + \hat{y}r_3, \\ \theta = (1 - \hat{x} - \hat{y})\theta_1 + \hat{x}\theta_2 + \hat{y}\theta_3, \\ x = r \cos \theta; y = r \sin \theta. \end{cases} \quad (2.10)$$

Then $T = F_T(\hat{T})$ defines a curved triangular element as shown in Figure 3(b).

The k -th order polynomials $P_k(\hat{T})$ defined on the reference finite element \hat{T} may be taken as the shape functions \hat{P} , for example, we may set $\hat{P} = P_2(\hat{T})$. In our numerical experiments, the reference finite element triple $(\hat{T}, \hat{P}, \hat{\Sigma})$ [14], which is a quadratic Lagrange finite element, is taken as

$$\begin{cases} \hat{T} \text{ is the reference triangular element shown in Figure 3(a),} \\ \hat{P} = P_2(\hat{T}), \\ \hat{\Sigma} = \{\hat{p}(\hat{a}_i), 1 \leq i \leq 3; \hat{p}(\hat{a}_{ij}), 1 \leq i < j \leq 3\}, \end{cases} \quad (2.11)$$

where \hat{a}_i denotes the vertexes of the reference triangular element (see Figure 3(a)), and \hat{a}_{ij} denotes the midpoint between \hat{a}_i and \hat{a}_j .

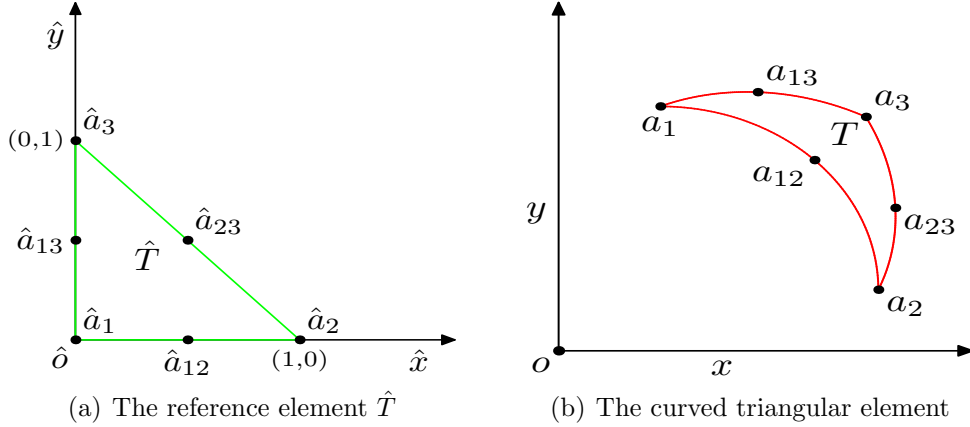


Figure 3: Parametric element with polar coordinates.

The dual-parametric finite element is now defined as a finite element triple [14] (T, P_T, Σ) by

$$\begin{cases} T = F_T(\hat{T}) \text{ is the curved triangle element,} \\ P_T = \{p : T \rightarrow \mathbb{R} \mid p = \hat{p} \circ F_T^{-1}, \forall \hat{p} \in \hat{P}\}, \\ \Sigma_T = \{p(a_i), 1 \leq i \leq 3; p(a_{ij}), 1 \leq i < j \leq 3\}. \end{cases} \quad (2.12)$$

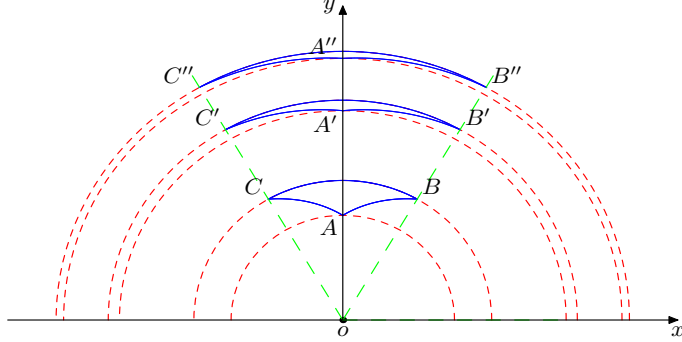


Figure 4: Dual-parametric element admit orientation preserving large expansionary deformations.

As is illustrated in Figure 4, the dual-parametric element permit extremely large orientation preserving expansionary deformations.

2.3. The finite element discretization and the algorithm

Let \mathcal{J}_h be a curved triangulation of the domain Ω_ε with the polar parametric elements, the dual parametric finite element function space is defined as

$$X_h := \{\mathbf{u}_h \in C(\bar{\Omega}_\varepsilon) : \mathbf{u}_h|_T \in P_T, \mathbf{u}_h(\mathbf{x}) = \mathbf{u}_0(\mathbf{x}), \forall \mathbf{x} \in \Gamma_0\}.$$

The corresponding homogeneous finite element function space is defined as

$$X_{h,0} := \{\mathbf{u}_h \in C(\bar{\Omega}_\varepsilon) : \mathbf{u}_h|_T \in P_T, \mathbf{u}_h(\mathbf{x}) = 0, \forall \mathbf{x} \in \Gamma_0\}.$$

For a finite element function $\mathbf{u}_h \in X_h$, the discrete energy $E_h(\mathbf{u}_h)$ is given by

$$E_h(\mathbf{u}_h) = \sum_{T \in \mathcal{J}_h} \sum_{j=1}^M W(\nabla \mathbf{u}_h(b_j)) \omega_{T,j},$$

where $b_j \in T$, $j = 1, \dots, M$ are the quadrature points, and $\omega_{T,j}$ are the corresponding quadrature weights. In our numerical experiments, $\omega_{T,j} = \omega_{\hat{T},j} \det(\nabla F_T(\hat{b}_j))$ with $\omega_{\hat{T},j}$ being the weights of the 5-th order Gaussian quadrature on the reference element \hat{T} . This leads to the weak form of the discrete Euler-Lagrange equation

$$\sum_{T \in \mathcal{J}_h} \sum_{j=1}^M D_F W(\nabla \mathbf{u}_h(b_j)) : \nabla \mathbf{v}_h(b_j) \omega_{T,j} = 0, \quad \forall \mathbf{v}_h \in X_{h,0}. \quad (2.13)$$

For the stored energy density function given by (1.4), this gives

$$\sum_{T \in \mathcal{J}_h} \sum_{j=1}^M [|\nabla \mathbf{u}_h|^{p-2} \nabla \mathbf{u}_h : \nabla \mathbf{v}_h + h'(\det \nabla \mathbf{u}_h) \operatorname{adj} \nabla \mathbf{u}_h : \nabla \mathbf{v}_h] (b_j) \omega_{T,j} = 0, \quad \forall \mathbf{v}_h \in X_{h,0}. \quad (2.14)$$

We apply a modified Picard iteration scheme to numerically solve the discrete Euler-Lagrange equation, that is to solve the following equation iteratively

$$\begin{aligned} & \sum_{T \in \mathcal{J}_h} \sum_{j=1}^M [|\nabla \mathbf{u}_h^n|^{p-2} \nabla (\mathbf{u}_h^{n+1} - \mathbf{u}_h^n) : \nabla \mathbf{v}_h] (b_j) \omega_{T,j} = \\ & - \Delta t^n \sum_{T \in \mathcal{J}_h} \sum_{j=1}^M [|\nabla \mathbf{u}_h^n|^{p-2} \nabla \mathbf{u}_h^n : \nabla \mathbf{v}_h + h'(\det \nabla \mathbf{u}_h^n) \operatorname{adj} \nabla \mathbf{u}_h^n : \nabla \mathbf{v}_h] (b_j) \omega_{T,j}, \end{aligned} \quad \forall \mathbf{v}_h \in X_{h,0}, \quad (2.15)$$

where Δt^n is the step size which should be properly chosen so that the sequence produced by the iteration is physically admissible and has decreasing elastic energy. In computation, the physical admissibility is usually guaranteed by requiring $\det(\nabla \mathbf{u}(b_{T,j})) > 0$ for all $T \in \mathcal{J}_h$ and $1 \leq j \leq M$. The algorithm is summarized as follows:

- (1) Set the initial deformation \mathbf{u}_h^0 , set Δt^0 .
- (2) Solve the linear finite element equation (2.15) for $(\mathbf{u}_h^{n+1} - \mathbf{u}_h^n)$ to get \mathbf{u}_h^{n+1} ;
- (3) If $\det(\nabla \mathbf{u}_h^{n+1})$ is negative on any quadrature point or $E(\mathbf{u}_h^{n+1}) > E(\mathbf{u}_h^n)$, then halve the step size Δt^n and go to step 2; else, go to step 4.
- (4) If $\|\mathbf{u}_h^{n+1} - \mathbf{u}_h^n\|_{L^2(\Omega_\varepsilon)} < \Delta t^n \cdot \text{TOL}$, then output \mathbf{u}_h^{n+1} as the solution and stop; otherwise go to step 2.

3. Numerical examples

In our numerical experiments, we use the stored energy density function given in (1.4) with $p = 1.5$ and $h(\delta) = \frac{(\delta-1)^2}{2} + \frac{1}{\delta}$, take the expansionary parameter $\lambda = 2$ and the tolerance $\text{TOL} = 10^{-6}$. For the convenience of

comparison with analytical and 1D numerical results on radially symmetric problems, we first concentrate on the regularized spherical reference domain

$$\Omega_\varepsilon = \{\mathbf{x} \in \mathbb{R}^n : \varepsilon < |\mathbf{x}| < 1\}. \quad (3.16)$$

We introduce curved triangulations on Ω_ε by the polar coordinates parametric elements defined in Section 2.2 (see (2.10)). Figure 5(a) shows a typical radially symmetric curved triangulation so produced on Ω_ε with $\varepsilon = 0.01$, while Figure 5(b) shows the final numerical solution obtained by our algorithm, which is perfectly symmetric as in contrast to the screwed numerical solution (see Figure 2) produced by the piecewise affine finite element method. The converge behavior of the total elastic energy and the radius of the cavity of our algorithm, with respect to the iteration numbers n , is shown in Figure 6(a) and Figure 6(b) respectively.

Table 3 shows the convergence rates of the error of the cavity radius $\text{err}(r_h^{\text{cav}}(\Omega_\varepsilon))$, the error of the deformation in L^2 norm $\|\mathbf{u}_h - \mathbf{u}\|_{L^2(\Omega_\varepsilon)}$ and the error of the total elastic energy $\text{err}(E(\mathbf{u}_h))$ with respect to the mesh size, where the numerical solution obtained by a reduced 1D model with 160 nodes is taken as the real solution of the problem, and the meshes are uniformly refined with the mesh size reduced by a factor of 1/2, and thus the corresponding number of elements N_{elem} is increased by a factor of 4, in each refinement step.

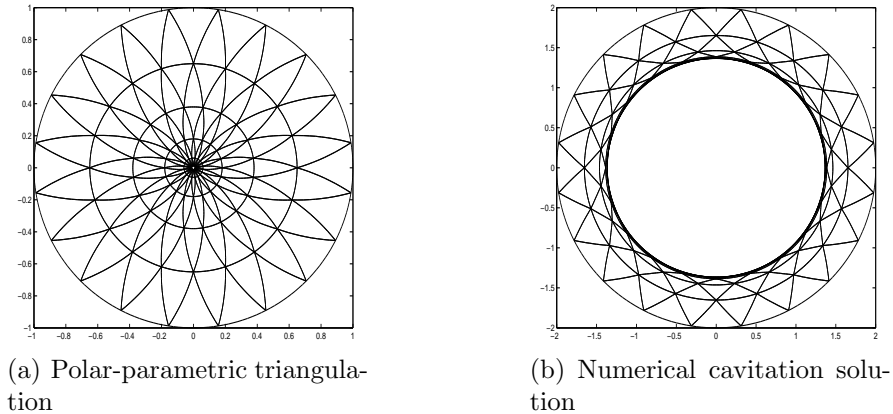
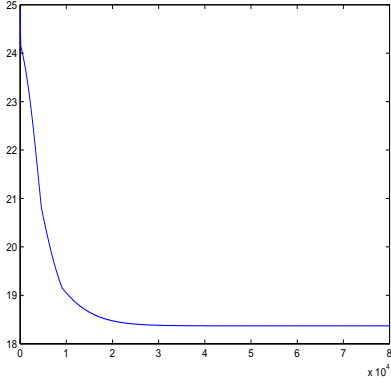
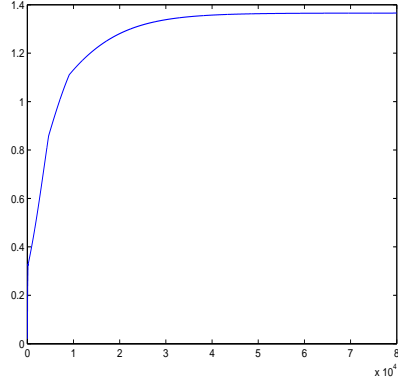


Figure 5: Dual-parametric mesh and cavitation solution with $\varepsilon = 0.01$.

Next, we explore the convergence behavior of the numerical cavitation as $\varepsilon \rightarrow 0$. According to Sivaloganathan's result [5, 7], we expect the numerical



(a) Energy converges decreasingly.



(b) Cavity radius converges increasingly.

Figure 6: The convergence behavior of the iteration process for $\varepsilon = 0.01$.

N_{elem}	$\text{err}(r_h^{\text{cav}}(\Omega_\varepsilon))$	rates	$\ \mathbf{u}_h - \mathbf{u}\ _{L^2(\Omega_\varepsilon)}$	rates	$\text{err}(E(\mathbf{u}_h))$	rates
40	2.9127e-02		2.2925e-02		4.3180e-01	
160	8.2114e-03	1.8273	7.8806e-03	1.5405	2.0770e-01	1.0559
640	2.6563e-03	1.6027	2.4383e-03	1.6924	6.9600e-02	1.5773
2560	5.1773e-04	2.3827	4.7775e-04	2.3516	1.4100e-02	2.3034

Table 1: The errors and the corresponding convergence rates with $\varepsilon = 0.01$.

cavitation solution \mathbf{u}_h^ε converges as $\varepsilon \rightarrow 0$, in particular, the cavity radius $r_h^{\text{cav}}(\Omega_\varepsilon)$ should converge to a positive number r_h^{cav} as $\varepsilon \rightarrow 0$. Figure 7(a) and Figure 7(b) show the numerical cavitation solutions $\mathbf{u}_h(\Omega_\varepsilon)$ for $\varepsilon = 0.1$ and $\varepsilon = 10^{-9}$ respectively. Table 2 demonstrates the convergence of the radius of the cavity $r_h^{\text{cav}}(\Omega_\varepsilon)$, and the convergence rate is closed to 1 as is shown in Figure 8. It is worth pointing out here that, in our computation, the pre-existing hole can be almost arbitrarily small, on the other hand, to our knowledge, there was no report on successful attempt, regardless of accuracy, on the cavitation computation for $\varepsilon \leq 10^{-3}$ before.

ε	1.0e-01	1.0e-02	1.0e-03	1.0e-04	1.0e-05
$r_h^{\text{cav}}(\Omega_\varepsilon)$	1.467498	1.367605	1.342616	1.339314	1.338971
ε	1.0e-06	1.0e-07	1.0e-08	1.0e-09	1.0e-10
$r_h^{\text{cav}}(\Omega_\varepsilon)$	1.338937	1.338934	1.338933	1.338933	1.338933

Table 2: Convergence of $r_h^{\text{cav}}(\Omega_\varepsilon)$ as $\varepsilon \rightarrow 0$.

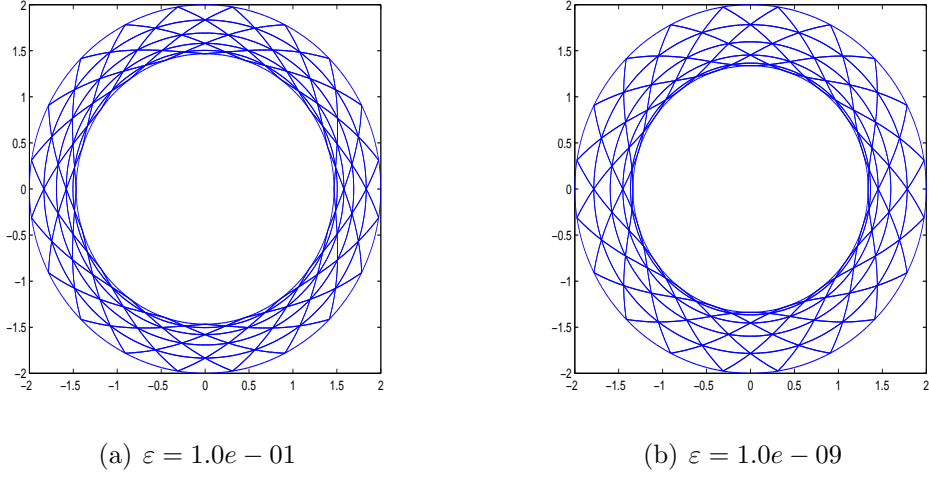


Figure 7: The numerical cavitation solutions $\mathbf{u}_h(\Omega_\varepsilon)$ for $\varepsilon = 0.1$ and $\varepsilon = 10^{-9}$.

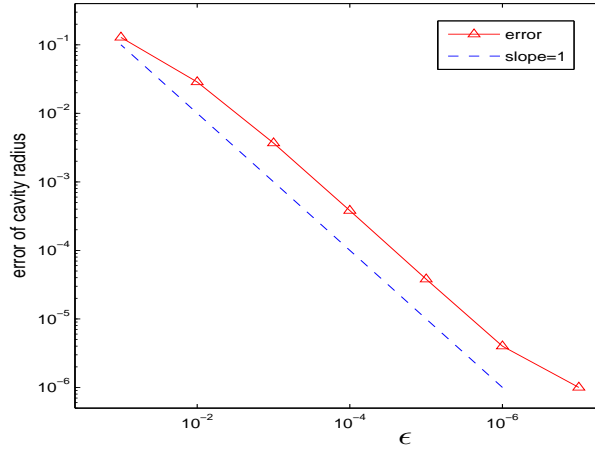


Figure 8: Convergence rate of $|r_h^{cav}(\Omega_\varepsilon) - r_h^{cav}|$ as $\varepsilon \rightarrow 0$.

To verify the applicability of our method to more general settings, we apply our method on a nonuniform asymmetric mesh with 2008 elements defined on Ω_ε with $\varepsilon = 0.01$ as shown in Figure 9(a), which is obtained by first applying the EasyMesh software to create a partition on the domain $\Omega' = \{\mathbf{y} \in \mathbb{R}^d : 1 < |\mathbf{y}| < 2\}$ with specified evenly spaced 128 nodes on the interior boundary and 64 nodes on the exterior boundary, and then map the

mesh to Ω_ϵ by the symmetric transformation $\mathbf{x} = (0.99(|\mathbf{y}| - 1) + 0.01)\frac{\mathbf{y}}{|\mathbf{y}|}$. Figure 9(b) shows the corresponding numerical cavitation solution, which agrees well with the one obtained on a symmetric mesh. In fact, the relative error of the cavitation radius is no more than 10^{-5} , which is of the same order with the corresponding symmetric counterpart.

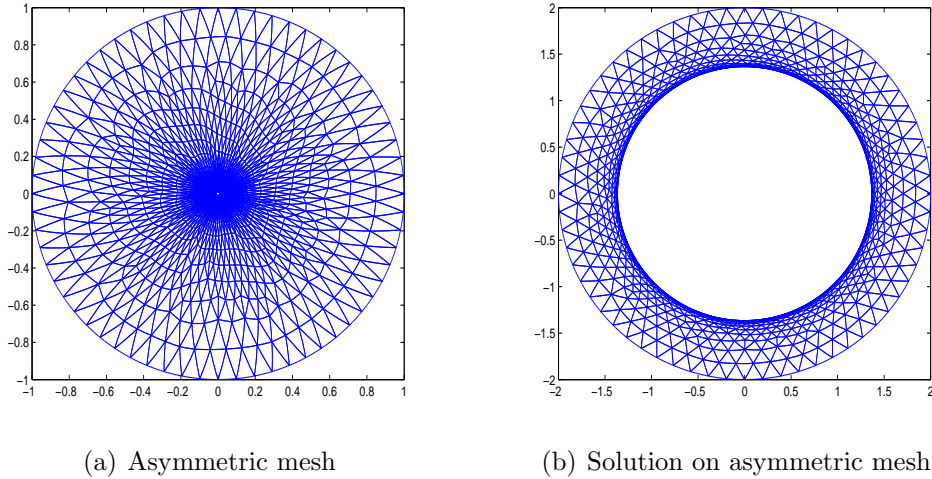


Figure 9: Solution on asymmetric mesh

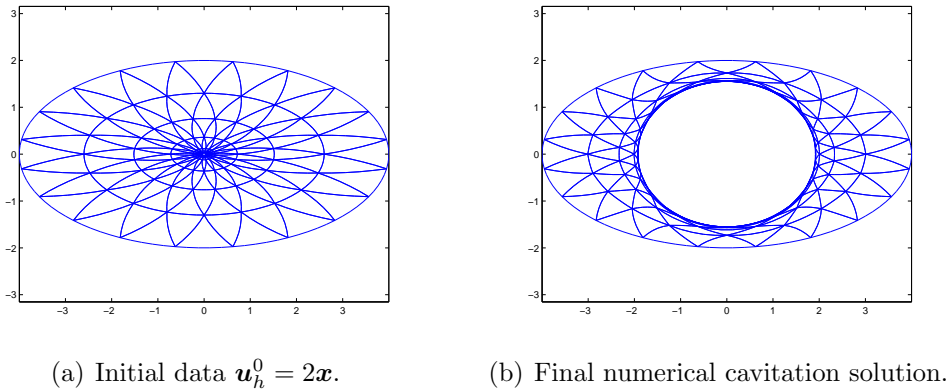


Figure 10: Example of an elliptic ring cavitation.

Last but not least, we replace the circular ring shaped reference configuration with $\epsilon = 0.01$ to an elliptic ring shaped one with the major axis

in coincidence with the x -axis and stretched by a factor of 2. The initial deformation is given by $\mathbf{u}_h^0 = 2\mathbf{x}$ as shown in Figure 10(a), and a numerical cavitation solution nicely produced by our algorithm is shown in Figure 10(b).

4. Conclusion

A dual-parametric curved triangular finite element method is introduced in this paper to numerically solve the cavitation problem. The method turns out to be a great success in the cavitation computation, thanks to the fact that the dual-parametric curved triangular finite element can very well fit the large expansionary deformation and is computationally stable. In fact, our numerical experiments show that, for a given initial circular hole with the radius ε as small as 10^{-10} , a highly accurate numerical cavitation can be produced with our method, which to our knowledge is the first successful numerical attempt of any kind reported in the existing literature for $\varepsilon \leq 10^{-3}$. Our numerical experiments also show that the method is highly efficient in the sense that a cavity developed from a very tiny (practically arbitrary small) deficiency can be captured quite accurately with only a small number of degrees of freedom. In addition, the method can be easily adapted to more general settings, and thus potentially provides a convenient tool to numerically study the mechanism of the cavitation phenomenon.

Acknowledgments

The AFEPack is used in our computation, we are grateful to Professor Ruo Li of Peking University to help us on the use of the software.

The research was supported by the Major State Basic Research Projects (2005CB321701), NSFC projects 10871011 and RFDP of China.

References

- [1] J. Ball, Discontinuous equilibrium solutions and cavitation in nonlinear elasticity, *Phil. Trans. Roy. Soc. London. A* 306 (1982), 557-611.
- [2] A. N. Gent, P. B. Lindley, International rupture of bonded rubber cylinders in tensions, *Proc. R. Soc. London. A* 249 (1958), 195-205.
- [3] S. Müller and S. J. Spector, An existence theory for nonlinear elasticity that allows for cavitation, *Arch. Rational Mech. Anal.* 131 (1995), 1-66.

- [4] P. V. Negrón-Marrero, O. Betancourt, The numerical computation of singular minimizers in two-dimensional elasticity, *J. Comp. Phys.* 113 (1994), 291-303.
- [5] J. Sivaloganathan, Uniqueness of regular and singular equilibria for spherically symmetric problems of nonlinear elasticity, *Arch. Rational Mech. Anal.*, 96 (1986), 97-136.
- [6] J. Sivaloganathan, S. J. Spector, On cavitation, configurational forces and implications for fracture in a nonlinearly elastic material, *J. Elasticity* 67 (2002), 25-49.
- [7] J. Sivaloganathan, S. J. Spector, V. Tilakraj, The convergence of regularized minimizers for cavitation problems in nonlinear elasticity, *SIAM J. Appl. Math.* 66 (2006), 736-757.
- [8] D. Henao, Cavitation, invertibility, and convergence of regularized minimizers in nonlinear elasticity, *J. Elasticity* 94 (2009), 55-68.
- [9] R. D. James, S. J. Spector, The formation of filamentary voids in solids, *J. Mech. Phys. Solids.* 39 (1991), 783-814.
- [10] J. Sivaloganathan, P. V. Negrón-Marrero, The numerical computation of the critical boundary displacement for radial cavitation, *Mathematics and Mechanics of Solids* 14 (2009), 696-726.
- [11] Xianmin Xu, Numerical simulation for microstructures of Large-body ferromagnetic materials, Doctorial dissertation, Peking University, Beijing, China, (2008), 84-106.
- [12] Xianmin Xu, D. Henao, A numerical Method for Cavitation in Nonlinear Elasticity, in preparation.
- [13] S. Biwa, Cavitation in finite elasticity with surface energy effects, *International Journal of non-linear mechanics*, 41 (2006), 1084-1094.
- [14] S. C. Brenner, L. R. Scott, The mathematical theory of finite element methods, Springer-Verlag, New York, (1994), 67-87.